

# Kinetics of Excitation Migration and Trapping in the Photosynthetic Unit of Purple Bacteria

Thorsten Ritz, Sanghyun Park, and Klaus Schulten\*

Beckman Institute, University of Illinois at Urbana-Champaign, 405 North Mathews Avenue, Urbana, Illinois 61801

Received: March 19, 2001; In Final Form: June 14, 2001

Purple bacteria have developed an efficient apparatus to harvest sunlight. The apparatus consists of up to four types of pigment–protein complexes: (i) the photosynthetic reaction center surrounded by (ii) the light-harvesting complex LH1, (iii) antenna complexes LH2, which are replaced under low-light conditions by (iv) antenna complexes LH3 with a higher absorption maximum. Following absorption of light anywhere in the apparatus, electronic excitation is transferred between the pigment–protein complexes until it is used for the primary photoreaction in the reaction center. We calculate, using Förster theory, all rates for the inter-complex excitation transfer processes on the basis of the atomic level structures of the pigment–protein complexes and of an effective Hamiltonian, established previously, for intracomplex excitations. The kinetics of excitation migration in the photosynthetic apparatus is described through a master equation which connects the calculated transfer rates to the overall architecture of the apparatus. For two exemplary architectures the efficiency, distribution of dissipation, and time evolution of excitation migration are determined. Pigment–protein complexes are found to form an excitation reservoir, in which excitation is spread over many chromophores rather than forming an excitation funnel in which excitation is transferred without detours from the periphery to the RC. This feature permits a high quantum yield of 83% to 89%, but also protects the apparatus from overheating by spreading dissipation over all complexes. Substitution of LH2 complexes by LH3 complexes or changing an architecture in which few LH2 (LH3) complexes are in contact with LH1 to an architecture in which all LH2 (LH3) complexes are in contact with LH1 increases the quantum yield up to 94% and decreases the degree to which dissipation is evenly distributed.

## Introduction

The photosynthetic unit (PSU) of purple bacteria is a nanometric molecular machinery in which several hundred bacteriochlorophylls (BChl's) and carotenoids (Car's) absorb light and convert the light energy into vectorial energy transfer and, subsequently, an electrostatic potential. Only very few BChl's in the primary reaction site, termed the photosynthetic reaction center (RC), participate in the electron-transfer reaction; most BChl's serve as antennae, collecting sun light and transferring its energy, in the form of electronic excitation, to the RC.

Long before the elucidation of the PSU structure, scientists have described excitation migration in photosynthetic systems as an incoherent hopping process<sup>1,2</sup> between individual pigment molecules with the RC as a trap which captures excitation. Evaluation of the time until excitation is first trapped by the RC poses a first-passage time problem,<sup>3</sup> which has been solved for various hypothetical model architectures of the PSU.<sup>4–8</sup> Common to all these models is the assumption that the PSU consists of many individual pigment molecules organized on a lattice.

The organization of pigments (BChl's, Car's) in the PSU of purple bacteria has recently become known through X-ray crystallography, electron microscopy, and molecular modeling.<sup>9–12</sup> This work revealed a considerably more complex architecture of BChl's than previously assumed. BChl's in the PSU are held in space through a protein scaffold. The complex of BChl's

and protein scaffold is named light-harvesting complex, of which up to three different kinds exist in purple bacteria. Light harvesting complex I (LH1) surrounds the RC and contains a ring aggregate of 32 BChl's referred to as B875 BChl's according to their main absorption band; LH1 is in turn surrounded by antenna LH2 complexes, each of which contains a ring aggregate of 16–18 closely coupled B850 BChl's and 8–9 additional, loosely coupled B800 BChl's. Under continuous low-light and/or low-temperature conditions, a third type of light-harvesting complex, LH3, is expressed in some species as a replacement for LH2.<sup>13,14</sup> LH3 is structurally similar to LH2, but the absorption maximum of the BChl aggregate lies at 820 nm. The arrangement of pigments in a minimal PSU, consisting of one LH1–RC complex, two LH2 complexes and one LH3 complex, is shown in Figure 1.

The elucidation of the structure of the different components of the PSU allows one, in principle, to evaluate through the application of quantum mechanics the electronic and optical properties of individual pigment–protein complexes as well as the rates of intra- and intercomplex excitation transfers.<sup>15,16</sup>

Much attention has been devoted to the prediction of the optical properties of the BChl aggregates in light harvesting complexes. The excitations of the closely coupled B875, B850, and B820 BChl aggregates in LH1, LH2, and LH3, respectively, are coherently delocalized exciton states. The extent of delocalization is a matter of intense debate, with estimates ranging from 2 BChl's to the entire ring aggregate.<sup>17–21</sup> In addition to optical properties, individual excitation transfer steps within the LH2 complex have been investigated, namely B800–B850

\* Corresponding author. E-mail: kschulte@ks.uiuc.edu.

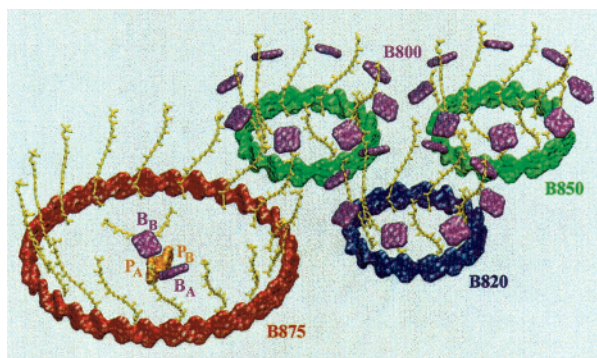


**Figure 1.** Arrangement of pigments in the photosynthetic unit of purple bacteria. The figure shows the pigments of one LH1–RC complex (left), two LH2 complexes (top right), and one LH3 complex (bottom right). Carotenoids are shown in yellow licorice representation, BChl's are shown in surface representation and are colored according to the energy of their absorption maxima, with colors shifted to the blue side of the visible spectrum for increasing energies. B800 BChl's in LH2 and accessory BChl's ( $B_A$ ,  $B_B$ ) in the RC are in purple, the B820 BChl ring in LH3 in blue, B850 BChl rings in LH2 in green, the B875 BChl ring in LH1 in red and the RC special pair BChl's ( $P_A$ ,  $P_B$ ) in the RC in orange. Produced with the program VMD.<sup>55</sup>

transfer<sup>22–25</sup> and carotenoid-BChl transfer.<sup>23,26,27</sup> The theoretical studies are paralleled by experimental studies, which are reviewed, e.g., in refs 28–31. These studies show that B800 BChl's and carotenoids transfer excitation within less than 1 ps to the B850 BChl system. Virtually no back-transfer from B850 BChl's occurs to the B800 BChl's or carotenoids. Carotenoids and B800 BChl's thus act as accessory pigments, which extend the spectral range of light absorption within one pigment–protein complex. However, they play no role in transferring excitation between different pigment–protein complexes.

In contrast to intra-complex excitation transfer, the inter-complex excitation transfer steps  $LH2 \leftrightarrow LH2$ ,  $LH2 \leftrightarrow LH1$ , and  $LH1 \leftrightarrow RC$  have been studied comparatively little, although these transfer steps account for the major amount of time spent in transferring excitation to the RC and, thus, determine the efficiency and dynamics of the excitation trapping process in the PSU.

In earlier work<sup>22,32</sup> we have introduced an effective Hamiltonian to describe the quantum states of the B850 and B875 BChl aggregates in LH2 and LH1 as exciton states delocalized over the complete BChl aggregates and have calculated transfer rates through a first-order perturbation theory scheme. More appropriate is a description of excitation transfer as an incoherent process,<sup>33</sup> for which the rates can be calculated with Fermi's Golden Rule. We have used this approach to calculate excitation transfer rates for the  $Car \leftrightarrow BChl$ ,  $B800 \leftrightarrow B850$ ,<sup>23</sup> and the  $LH1 \leftrightarrow RC$  steps.<sup>34</sup>

In this article, we evaluate the transfer rates for all inter-complex steps, namely  $LH2 (LH3) \leftrightarrow LH2 (LH3)$ ,  $LH2 (LH3) \leftrightarrow LH1$ , and  $LH1 \leftrightarrow RC$ . We assume that excitation is delocalized over the complete BChl aggregates involved and calculate rates according to Fermi's Golden Rule. For LH1 we consider, next to a complete circular aggregate as proposed previously,<sup>12</sup> also an alternative structure that consists of only part of a ring as suggested by electron microscopy.<sup>35</sup>

The availability of all rates for the different possible excitation transfer steps allows one to study the kinetics of excitation migration in the PSU of purple bacteria. After absorption of light in one of the pigment–protein complexes, excitation migrates between different pigment–protein complexes, until it either reaches an RC and delivers the energy to electron

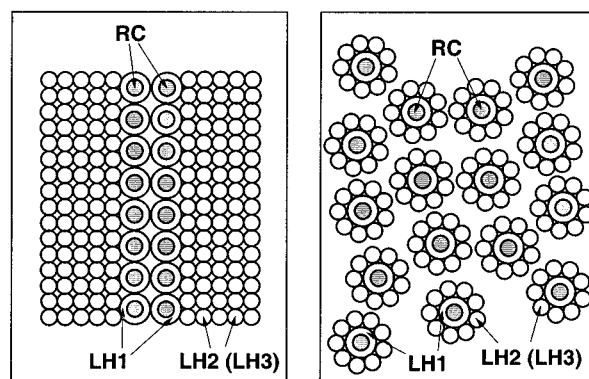


**Figure 2.** Schematic figures of the model architectures described in the text. Left: stripe architecture. Right: circular architecture.

transfer or dissipates its energy somewhere in the system. It has been observed that excitation is trapped in the RC 60–120 ps after absorption of light and that it is converted into electron transfer with a quantum yield of 95%.<sup>29,30</sup>

The *in vivo* architecture of the PSU, i.e., the stoichiometry and arrangement of the various pigment–protein complexes in the photosynthetic membrane, is not known with certainty. We study for the case of model architectures of the PSU, how sensitively excitation trapping depends on the architecture of the PSU and through which architectures a fast excitation trapping with a near unit quantum yield can be accomplished.

To guide our choice of model architectures from a huge number of possibilities, we use the following assumptions and experimental results. We assume that the membrane is filled densely enough with pigment–protein complexes, so that clusters of LH1 and LH2 complexes are formed, i.e., the distance between any pair of adjacent pigment–protein complexes is always taken to be the distance for which the van der Waals interaction between the respective pigment–protein complexes is minimized. The stoichiometry between LH1 and LH2 rings has been estimated to lie between 1:3<sup>36</sup> and 1:10.<sup>37</sup> The more LH2 complexes exist, the more time will be spent in  $LH2 \leftrightarrow LH2$  transfer steps with a resulting increase in trapping time and decrease in quantum yield. In the present study, we consider PSU's with stoichiometries 1:9 and 1:10 of LH1:LH2.

We investigate two model architectures, the circular and the stripe architecture, depicted in Figure 2, which can be considered extreme cases of possible PSU arrangements. In the stripe architecture, LH1–RC complexes form a 2-fold array as suggested in ref 38. To each LH1, 10 LH2's (LH3's) are attached in the form of a  $2 \times 5$  structure. The stripe architecture is motivated by electron microscopy observations of native LH2-less membranes from the purple bacterium *Rhodospirillum rubrum*, which show that LH1–RC complexes form ordered chains.<sup>35</sup> Possible excitation transfers in the stripe architecture are between an LH1 and the RC inside it, between neighboring LH1's, between an LH1 and an adjacent LH2 (LH3), and between neighboring LH2's (LH3's). In the circular architecture, an LH1–RC complex is surrounded by 9 LH2's (LH3's) and is isolated from other LH1–RC complexes. The circular architecture corresponds to the model of Papiz et al.<sup>39</sup> Fluorescence induction measurements in the purple bacterium *Rhodospirillum rubrum* agree best with a circular architecture of the PSU for this bacterium.<sup>40</sup> Possible excitation transfers in the circular architecture are between an LH1 and the RC inside it, between an LH1 and an adjacent LH2 (LH3), and between neighboring LH2's (LH3's). Using the rates for the individual transfer steps in a master equation for both architectures, we calculate the overall trapping yield, the mean

relaxation time of excitation, and we determine where energy is dissipated in the PSU.

## Theory

**Excitation Transfer Rates.** We assume that the excitations of the BChl aggregates in RC, LH1, LH2, and LH3 can be described in terms of single BChl  $Q_y$  excitations

$$|\alpha\rangle = |\text{BChl}_1 \text{BChl}_2 \cdots \text{BChl}_\alpha^* \cdots \text{BChl}_{2N}\rangle, \quad \alpha = 1, 2, \dots, 2N \quad (1)$$

Here,  $\text{BChl}_\alpha^*$  describes the  $\alpha$ th BChl being in the  $Q_y$  excited state, whereas all the other BChl's are in the electronic ground state.  $2N$  is the number of BChl's in the aggregate, i.e., four in case of the special pair + accessory BChl aggregate in the RC, 16 in case of the B850 BChl aggregate in LH2 and the B820 BChl aggregate in LH3, and 24 or 32 in case of the B875 BChl aggregate in LH1.

An excited state  $|\tilde{n}\rangle$  of a BChl aggregate is then expressed as a linear superposition of the individual  $Q_y$  excitations  $|\alpha\rangle$ ,

$$|\tilde{n}\rangle = \sum_{\alpha=1}^{2N} c_{n,\alpha} |\alpha\rangle \quad (2)$$

The coefficients  $c_{n,\alpha}$  are obtained by solving the eigenvalue problem of a  $2N \times 2N$  effective Hamiltonian  $\langle \alpha | \hat{H} | \beta \rangle$ , which has been introduced earlier.<sup>22,32,34</sup> The effective Hamiltonian is defined as

$$\langle \alpha | \hat{H} | \alpha \rangle = \epsilon \quad (3)$$

$$\langle \alpha | \hat{H} | \alpha + 1 \rangle = v_1 \quad \alpha \text{ even} \quad (4)$$

$$\langle \alpha | \hat{H} | \alpha + 1 \rangle = v_2 \quad \alpha \text{ odd} \quad (5)$$

$$\langle \alpha | \hat{H} | \beta \rangle = C \left( \frac{\vec{d}_\alpha \cdot \vec{d}_\beta}{r_{\alpha\beta}^3} - \frac{3(\vec{r}_{\alpha\beta} \cdot \vec{d}_\alpha)(\vec{r}_{\alpha\beta} \cdot \vec{d}_\beta)}{r_{\alpha\beta}^5} \right) \quad \beta \neq \alpha, \alpha \pm 1 \quad (6)$$

Here,  $\epsilon$  denotes the excitation energy of the BChl  $Q_y$  state,  $v_1$  and  $v_2$  are the nearest neighbor coupling strengths,  $\vec{d}_\alpha$  are unit vectors describing the direction of the transition dipole moments of the ground state (g)  $\rightarrow Q_y$  state transition of the  $\alpha$ th BChl, and  $\vec{r}_{\alpha\beta}$  is the vector connecting the centers of BChl  $\alpha$  and BChl  $\beta$ .  $C$  is a parameter related to the oscillator strength of the g  $\rightarrow Q_y$  transition.

The parameters have been chosen, as suggested in ref 22, such that the effective Hamiltonian spectrum of LH2 matches as close as possible the spectrum of an extensive quantum chemistry calculation of LH2, reported in ref 41. For LH2, this results in the choice of parameters:  $\epsilon = 13059 \text{ cm}^{-1}$ ,  $v_1 = 806 \text{ cm}^{-1}$ ,  $v_2 = 377 \text{ cm}^{-1}$ , and  $C = 519\,044 \text{ Å}^3 \text{ cm}^{-1}$ . Geometry and direction of transition dipole moments are taken from the crystal structure of LH2 from *Rhodospirillum (Rs.) molis-chianum*. For LH3 and LH1 complexes,  $\epsilon$  is adapted such that the absorption maximum of the BChl aggregate lies at 820 and 875 nm, respectively, while all other parameters are taken as before.

In addition to LH2, we consider LH3 complexes, in which the BChl aggregate absorbs at 820 nm. The shift in absorption maximum implies that we need to choose  $\epsilon = 13489 \text{ cm}^{-1}$ . We assume that LH3 is structurally identical to LH2, which is supported by an X-ray crystallographic structure of LH3 from *Rps. acidophila* (Richard Cogdell, personal communication).

Excitation transfer between a donor and an acceptor pigment proceeds through an incoherent hopping process the rate of which can be calculated according to the expression<sup>1</sup>

$$k_{\text{DA}} = \frac{2\pi}{\hbar} |U_{\text{DA}}|^2 J_{\text{DA}}, \quad J_{\text{DA}} = \int \frac{S_{\text{D}}(E) S_{\text{A}}(E)}{E^4} dE \quad (7)$$

Here,  $U_{\text{DA}}$  denotes the electronic coupling between donor and acceptor states and  $J_{\text{DA}}$  represents the overlap of the emission spectrum  $S_{\text{D}}$  of the initially excited donor, normalized to 1 on an energy scale, with the absorption spectrum  $S_{\text{A}}$  of the finally excited acceptor.  $S_{\text{D}}$  and  $S_{\text{A}}$  are approximated by Gaussians with parameters  $E_{\text{D(A)}}$  [energy of maximum emission(absorption)] and  $\Gamma_{\text{D(A)}}$  [full width at half-maximum] estimated from experiments and calculations.<sup>22,34</sup>

The coupling between the  $m$ th excited state of the donor BChl aggregate and the  $n$ th excited state of the acceptor BChl aggregate can be expressed as follows

$$U_{\text{DA}} = \langle \tilde{m} | \hat{V} | \tilde{n} \rangle = \sum_{\alpha=1}^{2N} \sum_{\beta=1}^{2M} c_{m,\alpha} c_{n,\beta} V_{\alpha,\beta} \quad (8)$$

Here,  $c_{m,\alpha}$ ,  $c_{n,\beta}$  are the coefficients of the eigenfunctions for the BChl aggregate excitations, as defined in eq 2, and  $V_{\alpha,\beta}$  denotes the coupling between two individual BChl molecules, which is approximated as an induced dipole-induced dipole interaction term

$$V_{\alpha,\beta} = C' \left( \frac{\vec{d}_\alpha \cdot \vec{d}_\beta}{r_{\alpha\beta}^3} - \frac{3(\vec{r}_{\alpha\beta} \cdot \vec{d}_\alpha)(\vec{r}_{\alpha\beta} \cdot \vec{d}_\beta)}{r_{\alpha\beta}^5} \right) \quad (9)$$

Equation 9 is identical to eq 6 except for that the BChl's  $\alpha$  and  $\beta$  now belong to two different pigment-protein complexes and not to the same complex as in eq 6. While the complete parameter set of the effective Hamiltonian can only be determined through extensive quantum chemical calculations, the dipolar coupling strength  $C'$  can be determined through direct measurement of transition dipole moments of BChl molecules. Measured values range from 6.1 D<sup>42</sup> in organic solvent to 7.7 D in BChl *a* protein from *Prostheochloris aestuarii*.<sup>43</sup> We employ a value of 6.3 D as in ref 34 and a corresponding value of  $C' = 170\,342 \text{ Å}^3 \text{ cm}^{-1}$ .

To calculate the rate of excitation transfer between BChl aggregates, we assume that an equilibrium between the donor excited states is established, so that the donor excited states are populated according to the Boltzmann distribution. The rate of excitation transfer between the donor excited state  $|\tilde{m}\rangle$  and acceptor excited state  $|\tilde{n}\rangle$  is

$$k_{\text{DA}} = \frac{2\pi}{\hbar} \sum_m \sum_n \frac{e^{-E_m/kT}}{\sum_m e^{-E_m/kT}} |U_{\text{DA}}|^2 \int \frac{S_m(E) S_n(E)}{E^4} dE \quad (10)$$

with  $U_{\text{DA}}$  as defined in eqs 8 and 9.

**Master Equation.** To describe the excitation migration in the PSU, which is a stochastic process, we set up a master equation connecting the architecture to the rates. First, we label all sites (pigment-protein complexes) with integers running from 1 to  $M$ . The probability  $p_i(t)$  that the site  $i$  is excited at time  $t$  satisfies the master equation:

$$\partial_t p_i(t) = \sum_{j=1}^M [W_{ij} p_j(t) - W_{ji} p_i(t)] \quad (11)$$



where  $W_{ij}$  is the transition rate from site  $j$  to site  $i$ . If, for example, site  $i$  is an LH1 and site  $j$  is an LH2 adjacent to site  $i$ ,  $W_{ij}$  takes the value of the excitation transfer rate from an LH2 to an LH1. By defining the rate matrix  $\mathcal{K}$  through its matrix elements  $\mathcal{K}_{ij} \equiv W_{ij} - \delta_{ij} \sum_k W_{kj}$ , the master equation 11 can be cast into a compact form

$$\partial_t |p(t)\rangle = \mathcal{K} |p(t)\rangle \quad (12)$$

where  $|p(t)\rangle$  is the column vector of  $p_i(t)$ 's. To incorporate dissipation and electron transfer, we subtract the dissipation rate from all diagonal elements of the rate matrix  $\mathcal{K}$  and the electron-transfer rate from the diagonal elements corresponding to RC's. Given an initial state  $|p(0)\rangle$ , the unique solution of the differential equation 12 is

$$|p(t)\rangle = e^{\mathcal{K}t} |p(0)\rangle \quad (13)$$

To understand how well the molecular machinery of the PSU works in trapping light energy, we ask the following three questions: What is the efficiency? (What fraction of the excitation energy is delivered to the electron transfer?) Is the dissipation spread out evenly so that no part of the system can get burnt? What is the time scale of the entire trapping process?

As a measure of the efficiency, we define the *yield*  $q(j)$  to be the probability that the excitation energy is used in the electron transfer when the site  $j$  is excited initially ( $|p(0)\rangle = |e_j\rangle$ , where  $|e_j\rangle$  is the column vector that has a one at site  $j$  and zeros elsewhere). Between time  $t$  and  $t + dt$ , the excitation energy is used in the electron transfer with the probability  $dt k_{et} \langle \text{RC} | p(t) \rangle$ , where  $k_{et}$  is the electron-transfer rate and  $\langle \text{RC} |$  is the row vector that has ones at sites for RC's and zeros elsewhere. This instantaneous probability is integrated over time to give the yield:

$$q(j) = \int_0^\infty dt k_{et} \langle \text{RC} | p(t) \rangle = \int_0^\infty dt k_{et} \langle \text{RC} | e^{\mathcal{K}t} | e_j \rangle \quad (14)$$

where we used the solution 13.

To investigate whether the dissipation is spread out evenly throughout the system, we choose an initial state in which the excitation probability is equally distributed at all sites ( $|p(0)\rangle = M^{-1} |1\rangle$ , where  $|1\rangle$  is the column vector whose elements are all ones and  $M$  is the number of sites). We then define the *dissipation*  $d(j)$  to be the probability that the excitation energy is dissipated at site  $j$ . Between time  $t$  and  $t + dt$ , the probability that the excitation energy is dissipated at site  $j$  is  $dt k_{diss} \langle e_j | p(t) \rangle$ , where  $k_{diss}$  is the dissipation rate which is assumed to be the same for all kinds of the pigment–protein complexes. Integrating over time, one obtains

$$d(j) = \int_0^\infty dt k_{diss} \langle e_j | p(t) \rangle = \int_0^\infty dt k_{diss} \langle e_j | e^{\mathcal{K}t} M^{-1} | 1 \rangle \quad (15)$$

The time scale of the entire trapping process is not such a straightforward concept as the efficiency or the dissipation. We measure the time scale via a monoexponential approximation of excitation decay. We take the initial state  $|p(0)\rangle = |e_j\rangle$  and consider the quantity

$$n(t) \equiv \langle 1 | p(t) \rangle \quad (16)$$

which is the probability that the system remains excited at time  $t$ . Since this probability is initially equal to one and eventually decays to zero, we approximate it by an exponential function  $e^{-t/\tau(j)}$ . The *mean relaxation time*  $\tau(j)$ , which depends on the initially excited site  $j$ , serves as a measure of the time scale of

the trapping process. We determine  $\tau(j)$  by requiring that the monoexponential approximation gives the correct integral:

$$\int_0^\infty dt e^{-t/\tau(j)} = \int_0^\infty dt n(t) \quad (17)$$

Since the left-hand side is equal to  $\tau(j)$ , it follows that

$$\tau(j) = \int_0^\infty dt \langle 1 | p(t) \rangle = \int_0^\infty dt \langle 1 | e^{\mathcal{K}t} | e_j \rangle \quad (18)$$

One can notice that the formulas 14, 15, and 18 for the yield, dissipation, and mean relaxation time, respectively, are all in the form of  $\int_0^\infty dt \langle \phi | e^{\mathcal{K}t} | \psi \rangle$ . Since this integral is equal to  $-\langle \phi | \mathcal{K}^{-1} | \psi \rangle$ , where  $\mathcal{K}^{-1}$  denotes the inverse of the rate matrix  $\mathcal{K}$ , we obtain

$$q(j) = -k_{et} \langle \text{RC} | \mathcal{K}^{-1} | e_j \rangle \quad (19)$$

$$d(j) = -k_{diss} M^{-1} \langle e_j | \mathcal{K}^{-1} | 1 \rangle \quad (20)$$

$$\tau(j) = -\langle 1 | \mathcal{K}^{-1} | e_j \rangle \quad (21)$$

## Results

**Excitation Transfer Times.** We calculate excitation transfer times for the inter-complex transfer steps, LH2 (LH3)  $\leftrightarrow$  LH2 (LH3), LH2 (LH3)  $\leftrightarrow$  LH1, LH1  $\leftrightarrow$  RC. The distance between the respective pigment–protein complexes is not known, except for LH1 and RC. We arranged pigment–protein complexes such that the van der Waals interaction between complexes is minimized, resulting in a shortest Mg–Mg distance of about 24 Å between neighboring LH2's (LH3's) and 22 Å between LH1 and LH2 (LH3). The coordinates for this arrangement are provided in ref 22.

For LH2, we employ the complex from *Rs. molischianum* with 16 B850 BChl's.<sup>11</sup> For LH1, we consider two geometries, both based on the model reported in ref 12. In the closed LH1 geometry, we assume a complete ring of 32 BChl's. In the open LH1 geometry, we assume that only 24 BChl's are arranged on a ring segment with the same diameter as the closed ring, but only spanning two-thirds of a full circle. The latter arrangement was suggested through electron microscopy data of LH2-less membranes from *Rb. sphaeroides*.<sup>35</sup>

The spectra of exciton states in LH2 and LH1 have been reported earlier.<sup>22,32</sup> Here, we only recapitulate the main properties. A ring aggregate of  $N$  BChl's has  $N$  exciton states. In case that the transition dipole moments lie in the plane of the ring, the lowest energy exciton state with energy  $E_1$  is optically forbidden; the only states with large oscillator strength are the degenerate pair of exciton states at energies  $E_2$  and  $E_3$ . In case that the ring symmetry is broken, the degeneracy between the states  $|2\rangle$  and  $|3\rangle$  is lifted, and state  $|3\rangle$  donates oscillator strength to the lowest exciton state, which thus becomes optically allowed.

Excitation transfer between two adjacent LH2 complexes proceeds mainly through the optically allowed exciton states  $|2\rangle$ ,  $|3\rangle$ . Using eqs (10, 8, and 9), we calculate a transfer rate of 1/10.0 ps.

Excitation transfer from LH2 to LH1 occurs through a combination of several pathways. The dominant pathways are listed in Table 1. It is remarkable that many pairs of donor and acceptor states exhibit similar couplings. The key factor that determines which pathways are dominant is the population of the donor exciton states. Donor exciton states  $|4\rangle$ ,  $|5\rangle$  and higher exhibit couplings and spectral overlaps to acceptor exciton states, which are of a similar size as the lower-lying exciton states,

**TABLE 1: LH2 → LH1 Singlet Excitation Transfer: Coulomb Couplings  $U_{DA}$  (in  $\text{cm}^{-1}$ ), Spectral Overlap Integrals  $J_{DA}$  (in  $10^{-4}$  cm), and Rates  $k_{DA}$  (in 1/ps) for Transfer Pathways with Associated Rates Larger than 1/1000  $\text{ps}^a$** 

LH2 Exciton	Population	LH1 Exciton	$U_{DA}$	$J_{DA}$	$k_{DA}$
Closed LH1 Ring					
1	63.6%	2,3	1.6	14.4	1/349.8
1	63.6%	4,5	1.8	13.2	1/332.3
2,3	32.7%	1	2.6	4.3	1/867.7
2,3	32.7%	2,3	8.3	6.9	1/54.1
2,3	32.7%	4,5	9.5	13.1	1/21.7
2,3	32.7%	6,7	8.4	14.2	1/26.1
2,3	32.7%	8,9	6.4	6.8	1/92.7
4,5	3.2%	8,9	8.5	13.4	1/280.0
$\Sigma$ LH2		$\Sigma$ LH1			1/7.7
Open LH1 Ring					
2,3	32.7%	2	5.7	8.0	1/100.7
2,3	32.7%	3	8.8	12.2	1/27.5
2,3	32.7%	4	5.3	14.1	1/65.9
2,3	32.7%	5	8.1	12.9	1/30.4
$\Sigma$ LH2		$\Sigma$ LH1			1/7.7

<sup>a</sup> Electronic couplings are calculated in the dipolar approximation (see eq 9) assuming a value of 6.3 D for the transition dipole moment of BChl  $Q_y$  states. Couplings to exciton states are calculated according to expression 8 using the effective Hamiltonian described above.

but their low population precludes noticeable excitation transfer. Of the three lowest lying donor exciton states, the optically allowed states  $|\tilde{2}\rangle$ ,  $|\tilde{3}\rangle$  are coupled stronger than the forbidden state  $|\tilde{1}\rangle$ . Consequently, LH2 → LH1 excitation transfer is dominated by the pathways from the donor states  $|\tilde{2}\rangle$ ,  $|\tilde{3}\rangle$  to the acceptor states with the largest spectral overlap, i.e., to the states  $|\tilde{4}\rangle$ ,  $|\tilde{5}\rangle$  and  $|\tilde{6}\rangle$ ,  $|\tilde{7}\rangle$ .

Opening of the LH1 ring has no effect on the overall LH2 → LH1 transfer rate. While it is certainly coincidental that the overall transfer rate from LH2 to closed and open LH1 are exactly identical, namely 1/7.7 ps, the similar values of electronic couplings for different pairs of exciton states suggest that the overall LH2 → LH1 transfer rates should be similar as long as the highly populated donor LH2 exciton states remain in resonance with an acceptor LH1 exciton state. Twenty-four as well as 32 LH1 exciton states form both a quasi-continuum which ascertains sufficient resonance of the LH2 states  $|\tilde{2}\rangle$ ,  $|\tilde{3}\rangle$  with one of the LH1 exciton states.

The above result was obtained by placing the LH2 ring on the opposite side of the opening in the LH1 complex. If one moves the LH2 ring closer to the opening, the transfer rate slows down slightly.

Information regarding back-transfer from LH1 to LH2 is provided in Table 2. Because LH1 absorbs maximally at 875 nm and LH2 absorbs maximally at 850 nm, one expects back-transfer to be slower than forward transfer. In the case that all excitation in the BChl aggregates was located at two levels at 850 and 875 nm, respectively, one would predict, according to the detailed balance expression,

$$k_{D \leftarrow A} = e^{-\Delta E/kT} k_{D \rightarrow A} \quad (22)$$

that LH2 → LH1 back-transfer proceeds at a rate of 1/41 ps. The rate calculated with the effective Hamiltonian is, however, 1/15.5 ps for closed LH1 complexes. To explain this difference, one must note that excitation in BChl aggregates is distributed over several different exciton states. Between each pair of donor and acceptor excited states, the detailed balance condition (22) holds. However, if one reduces the multilevel exciton structure of the BChl aggregates to a simple two-level system, expression

**TABLE 2: LH1 → LH2 Singlet Excitation Transfer: Coulomb Couplings  $U_{DA}$  (in  $\text{cm}^{-1}$ ), Spectral Overlap Integrals  $J_{DA}$  (in  $10^{-4}$  cm), and Rates  $k_{DA}$  (in 1/ps) for Transfer Pathways with Associated Rates Larger than 1/1000  $\text{ps}^a$** 

LH1 exciton	Population	LH2 exciton	$U_{DA}$	$J_{DA}$	$k_{DA}$
Closed LH1 Ring					
1	33.3%	2,3	2.6	4.3	1/852.1
2,3	42.3%	1	1.6	14.4	1/526.0
2,3	42.3%	2,3	8.3	6.9	1/41.9
4,5	16.4%	4,5	9.5	13.1	1/43.4
4,5	16.4%	4,5	8.5	1.1	1/643.9
6,7	5.3%	2,3	8.4	14.2	1/161.2
6,7	5.3%	4,5	9.3	5.4	1/340.2
8,9	1.7%	4,5	8.5	0.2	1/527.1
$\Sigma$ LH1		$\Sigma$ LH2			1/15.5
Open LH1 Ring					
1	42.3%	2,3	4.3	5.2	1/207.5
2	25.5%	2,3	8.2	8.0	1/61.1
3	17.2%	2,3	6.1	12.2	1/110.3
4	6.6%	2,3	8.4	14.1	1/128.6
5	4.8%	2,3	5.4	12.9	1/464.2
$\Sigma$ LH1		$\Sigma$ LH2			1/20.3

<sup>a</sup> Electronic couplings are calculated in the dipolar approximation (see eq 9) assuming a value of 6.3 D for the transition dipole moment of BChl  $Q_y$  states. Couplings to exciton states are calculated according to expression 8 using the effective Hamiltonian described above.

22 yields an erroneous prediction of the ratio between forward and back-transfer rates. The effect of the exciton splitting in the BChl aggregates is thus to shift the LH2 ↔ LH1 transfer equilibrium to the side of LH2 as compared to a system in which no exciton exists and all excitation is localized on individual BChl's.

Back-transfer from the open LH1 complex is slightly slower than from the closed LH1 complex (in 20.3 instead of 15.5 ps). This effect is due to the differences in population of the exciton states in the open and closed geometries.

Excitation transfer between adjacent LH1 complexes was found to occur with a rate of 1/20.0 ps (complete LH1 rings). Transfer from LH1 to the RC has been calculated for the case of complete LH1 complexes in ref 34. A forward transfer rate of 1/14.5 ps and a back-transfer rate of 1/8.1 ps was found. Employing the method described in ref 34, we calculate for the open LH1 geometry a forward transfer rate of 1/29.3 ps and a back-transfer rate of 1/12.0 ps.

Finally, we investigate the inclusion of LH3 complexes in which the closely coupled BChl aggregate has an absorption maximum of 820 nm. We assume that LH3 is structurally identical to LH2, an assumption which is supported by an X-ray crystallographic structure of LH3 from *Rps. acidophila* (Richard Cogdell, personal communication). The calculations are identical to those presented above, except that the exciton levels of LH3 are shifted by 30 nm. Transfer between adjacent LH3 complexes occurs therefore with the same rate as transfer between neighboring LH2 complexes, namely with a rate of 1/10.0 ps. For LH3 ↔ LH2 transfer, we calculate a forward transfer rate of 1/11.3 ps and a back-transfer rate of 1/32.5 ps. For LH3 ↔ LH1 transfer, the calculated forward transfer rate is 1/14.0 ps and the back-transfer rate is 1/99.4 ps. As in the case of LH2 ↔ LH1 transfer, the ratio between forward and back-transfer rates for the LH3 ↔ LH2 and LH3 ↔ LH1 transfer steps is smaller than in the case of transfer between individual BChl's.

To summarize the results in this section, we present all calculated rates in Table 3.

**Excitation Migration.** We calculate the yield, dissipation, and mean relaxation time in the stripe and the circular

**TABLE 3: The Excitation Transfer Rates (in 1/ps) between Pigment–Protein Complexes as Calculated with the Effective Hamiltonian and Equations 8–10<sup>a</sup>**

to	from				
	RC	LH1 (closed)	LH1 (open)	LH2	LH3
RC		1/15.8	1/29.3		
LH1 (closed)	1/8.1	1/20.0		1/7.7	1/14.0
LH1 (open)	1/12.0			1/7.7	
LH2		1/15.5	1/20.3	1/10.0	1/32.5
LH3		1/99.4		1/11.3	1/10.0
dissipation rate = 1/1000.0					
electron-transfer rate = 1/3.0					

<sup>a</sup> Also shown are the dissipation rate and the electron transfer rate assumed in our calculations.

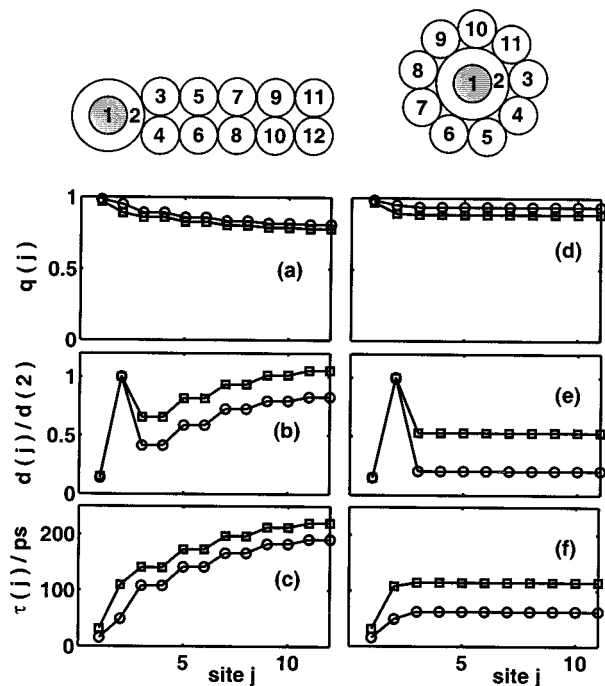


**Figure 3.** The yield  $q(j)$ , dissipation  $d(j)$ , and mean relaxation time  $\tau(j)$  of excitation migration for the stripe and the circular architecture. Top figures show the labeling of sites in each architecture. Left: stripe architecture. Right: circular architecture. Squares are for systems with LH2's and circles are for systems with LH3's. (a) and (d): The yield  $q(j)$ , i.e., the probability that the excitation energy is used in the electron transfer when site  $j$  is initially excited [see eqs 14 and 19]. (b) and (e): The dissipation  $d(j)$ , i.e., the probability that the excitation energy is dissipated at site  $j$  when the initial excitation is distributed equally at all sites [see eqs 15 and 20]. Dissipation is normalized with respect to the dissipation at the LH1 (site 2). (c) and (f): The mean relaxation time  $\tau(j)$  for the initial excitation at site  $j$  [see eqs 18 and 21].

architecture using eqs 19–21. For the stripe architecture, these observables turn out not to depend on the number of repeats of the single unit shown at the top of Figure 3, which consists of one RC, one LH1, and ten LH2's (LH3's). For the circular architecture, it is obvious that one can deal with only one single unit, which consists of one RC, one LH1, and nine LH2's (LH3's), because the circular units are isolated. Therefore, we plot in Figure 3 the observables for only one single stripe or circular unit, respectively.

The yield is shown in Figure 3a,d. Yield-wise the circular architecture is more favorable than the stripe architecture with a yield of 89% (circular) compared to 83% (stripe). The insertion of LH3's renders both architectures more efficient; however, the yield of the stripe architecture after insertion of LH3's (86%) is still smaller than the yield of the circular architecture with

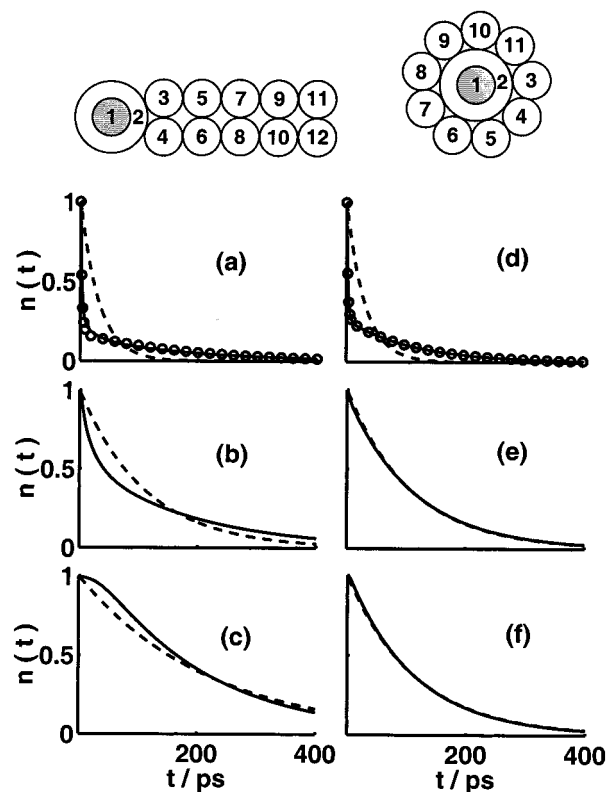


**Figure 4.** Time dependence of the excitation probability in the stripe and the circular architecture. Shown is the probability  $n(t)$  that any pigment in a system remains excited at time  $t$ . Left: stripe architecture with LH2's. Right: circular architecture with LH2's. (a) and (d): initial excitation at an RC. (b) and (e): initial excitation at an LH1 (site 2). (c) and (f): initial excitation at an LH2 (site 11). Solid lines: numerical integration of the differential eq 12. Dashed lines: monoexponential approximation. Circles in (a) and (d): biexponential approximation.

LH2's; in the latter case, the replacement of LH2's with LH3's raises the yield to 94%.

Since we are interested in how the dissipation is distributed throughout the system, relative dissipation rather than absolute dissipation is more appropriate to consider. As shown in Figure 3b,e, the dissipation is spread out more or less evenly throughout LH1's and LH2's while RC's are saved from dissipation. The latter result is mostly due to the fact that we considered the RC's to be in the "open" state, in which excitation is used within 3 ps to induce an electron transfer, leaving little time for dissipation in the RC's. If one considers "closed" RC's by setting  $k_{et}$  to zero, dissipation in the RC's is about five times higher than for "open" RC's (results not shown). With LH3's replacing LH2's, less energy is dissipated at the peripheral LH3 complex, resulting in a less even distribution of dissipation.

Figure 3c,f shows the mean relaxation time  $\tau(j)$ , corresponding to the assumption of monoexponential decay of excitation through electron transfer and dissipation.  $\tau(j)$  ranges from about 30 ps when an RC is excited initially to 100–200 ps when an LH2 is excited initially. Averaged over all pigment–protein complexes, the mean relaxation time is 168.8 ps in the stripe architecture and 106.5 ps in the circular architecture. If LH2's are replaced by LH3's, it decreases to 136.8 ps in the stripe architecture and to 56.9 ps in the circular architecture.

We also determined the actual time dependence of the relaxation of the excitation, calculating  $n(t)$  defined in eq 16 by a numerical integration of the differential equation 12. If the excitation starts at LH1 or LH2 (Figure 4b,c,e,f), the monoexponential approximation  $e^{-t/\tau}$ , where  $\tau$  is the mean relaxation



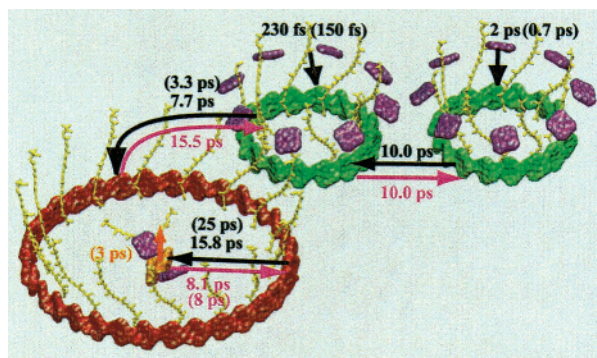


**Figure 5.** Excitation transfer times in the photosynthetic unit of purple bacteria. Values in parentheses indicate experimentally measured times, all the other values are calculated as described in the text. Produced with the program VMD.<sup>55</sup>

time as defined in eq 18, captures the overall time dependence of  $n(t)$  well. The time constants  $\tau$  for the graphs shown in Figure 4 are (b) 109.5 ps, (c) 219.9 ps (here, the LH2 complex most distant from the RC is initially excited), (e) 107.9 ps, and (f) 114.7 ps.

However, if an RC is excited initially (Figure 4a,d), the monoexponential decay does not describe the overall time dependence well. Although a large fraction of the excitation immediately leads to the electron transfer, still a significant fraction flows back to the LH complexes and decays slowly. Hence, there exist two different time scales for these two processes. To capture the two different time scales, one needs to assume a biexponential decay as derived in the appendix. In the stripe architecture, 83% of the excitation from the RC decays with a fast time constant  $\tau_1$  of 2.5 ps, and 17% decays with  $\tau_2 = 171.2$  ps (Figure 4a). In the circular architecture, 73% of the initial RC excitation decays with  $\tau_1 = 2.2$  ps and the remaining 27% with  $\tau_2 = 111.5$  ps (Figure 4d).

## Discussion

The photosynthetic unit is a nanometric molecular machinery built out of pigment–protein complexes, that are structurally known, while the organization of these complexes is not yet known. Through the application of quantum mechanics and using the known atomic geometries, we have calculated all transfer times (inverse of rates) between the different pigments in the PSU. These times are shown in Figure 5. The only empirical parameters entering our theoretical description are the shape and energy maxima of absorption and emission spectra as well as the transition dipole moment of the BChl  $Q_y$  transition.

The majority of the transfer times shown in Figure 5 have been presented in this article. In ref 23, we had evaluated B800  $\rightarrow$  B850 BChl transfer rates, albeit assuming a BChl  $Q_y$  transition dipole moment of 14.4 D. Assuming a transition dipole moment of 6.3 D, as used throughout the present article, the transfer rates scale with the factor  $(6.3/14.4)^4$  to a rate of 1/2.0 ps, which is stated in Figure 5. The transfer dynamics from carotenoids to BChl's is complex, involving several optically forbidden states of carotenoids; nevertheless, it is amenable to quantum mechanical evaluation.<sup>27,44</sup> Figure 5, presenting the complete set of transfer times, demonstrates a remarkable conceptional achievement, as it shows that a complex molecular machinery involving hundreds of pigments and tens of thousands of atoms can be described with accuracy through the application of the laws of quantum physics.

The calculated rates agree well, although not perfectly, with experimental results, indicated in parentheses in Figure 5. The experimentally determined B800  $\rightarrow$  B850 transfer rate is 1/700

fs<sup>45</sup> and 1/3.3 ps for LH2  $\rightarrow$  LH1 excitation transfer,<sup>46</sup> while no measurement exists for transfer between identical pigment protein complexes. One reason for the discrepancy between calculated and experimental rates can lie in an underestimation of the BChl  $Q_y$  transition dipole moment in the protein environment. We are not aware of a measurement of the BChl- $a$   $Q_y$  transition dipole moment in LH2 of purple bacteria, but we note that the BChl- $a$   $Q_y$  dipole moment of 7.7 D in the protein environment of *Prosthecochloris aestuarii* is larger than the value of 6.3 D in organic solvent, which we employed in our calculations. Assuming a value of 7.7 D, the calculated rates would increase by a factor of 2.2 and then yield excellent agreement with the experimental rates. An exception is the case of LH1  $\leftrightarrow$  RC excitation transfer, for which experimental estimates range from 1/35 ps to 1/50 ps for the forward and 1/8 ps to 1/12 ps for the back-transfer step.<sup>47–49</sup> The most likely reason for the faster calculated LH1  $\rightarrow$  RC transfer rates lies in an overestimate of the exciton delocalization. In the open LH1 geometry, in which excitation is delocalized over only 24 BChl's as compared to 32 BChl's in the closed LH1 geometry, LH1  $\rightarrow$  RC excitation transfer proceeds with a rate of 1/29.3 ps, a factor of 2 slower than for the closed LH1 complex. An even shorter delocalization length would result in a further slowing of the transfer rate.

The delocalization length depends on the presence of disorder. Static disorder, e.g., through inhomogeneities in the BChl binding sites, is found to have only a small effect on the quantum states and transfer rates.<sup>22,50,51</sup> A recent investigation<sup>52</sup> of the effect of dynamic disorder through thermal fluctuations on the quantum states and transfer rates suggests that dynamic disorder will reduce the delocalization length considerably.

Figure 5 reveals an important principle in the organization of the PSU. Forward and backward transfer rates between the different pigment–protein complexes are very similar and, thus, the transfer reactions are not biased strongly in any particular direction. In particular there exists no strong bias of excitation transfer toward the RC. It is therefore inappropriate to describe the BChl aggregates as forming an excitation funnel with the RC at the center. Only the accessory pigments, carotenoids and B800 BChl's funnel their excitation energy into the respective BChl aggregates. The system of BChl aggregates is better described as a reservoir in which excitation is distributed more or less evenly throughout the whole system. This organization appears to be rather inefficient. However, as shown in Figure 3, excitation is trapped within 200 ps or less at the RC, no matter which the initial site of excitation is. This mean relaxation time is small compared to the loss time of 1000 ps, so that the yield of the PSU remains high, namely above 85%.

The rationale for the reservoir picture becomes clear when one considers that RC's exist in two spectral forms. In the “open” form, the RC special pair is neutral and can utilize excitation toward an electron transfer. After the electron transfer, the RC is in the “closed” form with the active special pair BChl being in a cation state and unable to utilize further excitation until it is reduced by the uptake of an electron. Were the BChl aggregates in the LH1 and LH2 complexes forming an excitation funnel toward the RC, all of the excess excitation arriving while the RC is closed would be dissipated in the RC special pair, which could result in an overheating of the special pair. By lifting the energy of the RC above that of the B875 BChl aggregate in LH1, the back-transfer rate from the RC to LH1 becomes faster than the forward transfer rate from LH1 to the RC. If the RC is closed, excitation is returned to the LH1 complex, and thus, dissipation can be spread over a much larger

area. Dissipation is spread over an even larger area due to transfer from LH1 to LH2 complexes and subsequent transfer between LH2 complexes. As the calculation of the dissipation distribution shows (cf. Figure 3), the probability that excitation is dissipated in any of the LH2 complexes is between 50% and 110% (depending on the position of LH2 and the organization of the LH complexes) of the probability that excitation is dissipated in an LH1. This means that dissipation is effectively spread out over the entire BChl system. It appears to be more important for a purple bacterium to protect its PSU against damage from overheating than to gain an additional few percent in the yield. Only when the bacterium "starves" from a shortage of light through a long period of low irradiation, it changes the organization of its PSU. The LH2 complexes are replaced gradually by LH3 complexes which absorb at a higher energy. Under low-light and/or low-temperature conditions, all LH2 complexes are replaced by LH3.<sup>14</sup> The insertion of LH3 changes the excitation reservoir to an excitation funnel toward LH1. This change results in a reduction of the trapping time by about a factor of 2 and, consequently, in a rise of the yield from 83 to 86% in the stripe architecture and from 89 to 95% in the circular architecture. The price for the rise in yield is a more uneven distribution of dissipation.

It remains an open question how the LH complexes are organized into a PSU. However, we can investigate how the above-described functionality of the BChl system as an excitation reservoir or an excitation funnel with the resulting efficiency, trapping time and dissipation distribution depends on the organization of the PSU. We considered two extreme model architectures of the PSU. In the circular architecture, the distance from any LH2 to the RC is minimized, since each LH2 is in direct contact with LH1. In the stripe architecture, a similar number of LH2's are arranged in such a fashion that LH2's extend as far as possible away from the LH1-RC complex. Since we required that the architecture is densely filling the membrane, LH2's were arranged not in a single file but in a file of pairs extending up to five steps away from the LH1-RC complex. The trapping time in the circular architecture of about 110 ps is about a factor of 2 smaller than the trapping time in the stripe architecture. Consequently, the yield in the circular architecture is about 6–8% higher than in the stripe architecture. On the other hand, excitation is dissipated more evenly in the stripe architecture.

The changes in the observables from the stripe to the circular architecture are similar in quality and size as the changes that occur when LH2's are replaced by LH3's in any of the two architectures. Since the latter changes are important enough to be coded in the genome with the LH2/LH3 variability maintained over billions of years, we must conclude that the changes in the observables due to differences in architectures are also functionally important to the bacterium.

In the calculations of the quantities above, it has been assumed that all LH complexes are arranged at optimal inter-complex distances from each other as obtained from energy minimization. One may ask how the trapping time, yield, and dissipation distribution change if the distances between the LH complexes increase as would be the case in a less densely filled membrane, and whether the conclusions drawn above remain valid in this case. We have repeated the calculations, increasing all distances between LH complexes by up to 50 Å. The increased distance results in a longer transfer time between the complexes and consequently in a longer trapping time and a lower yield, while relatively more energy is dissipated in the LH2 (LH3) complexes. These changes in the functional proper-

ties for an increase in inter-complex distance parallel the changes that occur when changing from a circular to a stripe architecture. In fact, a circular architecture with all inter-complex distances increased by about 20 Å from the optimal values becomes virtually indistinguishable in its functional properties from a stripe architecture with optimal inter-complex distances. It is therefore not possible to identify the type of architecture employed on the basis of the functional properties alone. Knowledge of the distribution of inter-complex distances is required in addition. A first indication for the distribution of inter-complex distances would be how densely the membrane is filled, a value which may be amenable through measurements of the extinction coefficient and the molecular weight.

However, for any given distribution of inter-complex distances, the above-discussed differences in functional properties between circular and stripe architecture remain. In fact, they become more distinct for larger intercomplex distances. An increase of intercomplex distances by 10 Å in a system with LH2's results in an increase of trapping time from 107 to 125 ps in the circular architecture, while it increases the trapping time from 169 to 264 ps in the stripe architecture. The latter time and the corresponding low yield of 74% cannot be reconciled with experimental measurements, suggesting that purple bacteria do not employ a stripe architecture if their membrane is loosely filled with LH complexes.

It will be necessary to study whether changes from stripe to circular architectures do occur or whether the PSU is organized in a random architecture with functional properties lying between those of the stripe and circular architectures. Should the latter be the case, this would indicate that the expense for the bacterium to organize the PSU into a regular architecture is higher than the expense of replacing all LH2 complexes by a genetically modified LH3 complex in a random architecture. Should the former be the case, the question arises by which mechanism the reorganization of the PSU is accomplished. If the PSU assembles in a self-organized, diffusion controlled fashion, a reorganization can be accomplished by changing the interaction energies between LH1 and LH2 in relation to the interaction energy between LH2 complexes. One can, in principle, determine the interaction energies through molecular dynamics simulations with external forces or through atomic force microscopy and optical tweezer experiments.

If the PSU is assembled with the help of chaperones, studies are necessary to determine the nature of the chaperones and how they control the assembly of the PSU. In case of *Rs. rubrum* the PSU consists solely of the RC and LH1. The proteins are encoded by the *puf* and *puhA* operons that are accompanied by three flanking open reading frames (G115, I2372, I3087).<sup>53</sup> The latter codes for proteins are expressed at very low levels and may assist in the assembly of the PSU. In case of *Rhodobacter sphaeroides* the *pufX* gene was found to code for a protein that induces (i) a specific orientation of the RC in the LH1 ring and (ii) the formation of a regular array of LH1-RC complexes, likely by actually also preventing closure of the LH1 ring.<sup>38</sup>

The questions raised in the last two paragraphs point to a new type of problem which is prone to become more prominent in biophysics: In addition to the protein-folding problem (How does a polypeptide chain assume reproducibly a 3D structure?) and the structure-function-relation problem (How does the architecture of a system relate to its biological function?), it is necessary to understand the mechanism and dynamics of assembly of already folded proteins into multi-protein machineries. The PSU of purple bacteria is one of the largest structurally resolved multiprotein machineries and, as shown here, we are



able to predict functional properties of this machinery from its architecture. Beyond its importance as an example of an energy conversion machine, the photosynthetic unit is therefore likely to play a key role in unlocking the principles that govern the functionality of large-scale cellular machineries in general.

**Acknowledgment.** We are indebted to Sinan Arslan for contributing to this paper. His programming efforts have greatly facilitated the calculation of the excitation transfer rates presented here. We also would like to thank Ana Damjanović for her contributions. This work was supported by grants from the National Science Foundation (NRAC MCA93S028), the National Institutes of Health (NIH PHS 5 P41 RR05969), and the Roy J. Carver Charitable Trust.

## Appendix: Biexponential Approximation

We seek to approximate  $n(t) \equiv \langle 1|p(t) \rangle$  by a biexponential function,  $a_1 e^{-t/\tau_1} + a_2 e^{-t/\tau_2}$ , by matching four moments:<sup>54</sup>

$$\mu_0 \equiv n(0) = \langle 1|p(0) \rangle = 1 \quad (23)$$

$$\mu_1 \equiv -\partial_t n(0) = -\langle 1|\partial_t p(0) \rangle = -\langle 1|\mathcal{H}|p(0) \rangle \quad (24)$$

$$\mu_{-1} \equiv \int_0^\infty dt n(t) = \int_0^\infty dt \langle 1|e^{\mathcal{H}t}|p(0) \rangle = -\langle 1|\mathcal{H}^{-1}|p(0) \rangle \quad (25)$$

$$\mu_{-2} \equiv \int_0^\infty dt t n(t) = \int_0^\infty dt \langle 1|te^{\mathcal{H}t}|p(0) \rangle = \langle 1|\mathcal{H}^{-2}|p(0) \rangle \quad (26)$$

Imposing these four conditions on the biexponential function corresponds to

$$a_1 + a_2 = \mu_0 \quad (27)$$

$$a_1/\tau_1 + a_2/\tau_2 = \mu_1 \quad (28)$$

$$a_1\tau_1 + a_2\tau_2 = \mu_{-1} \quad (29)$$

$$a_1\tau_1^2 + a_2\tau_2^2 = \mu_{-2} \quad (30)$$

From this, one can determine the four unknowns,

$$\tau_{1,2} = 2A/(B \pm \sqrt{B^2 - 4AC}) \quad (31)$$

$$a_{1,2} = \pm(\tau_{2,1}^{-1}\mu_0 - \mu_1)/(\tau_2^{-1} - \tau_1^{-1}) \quad (32)$$

where

$$A \equiv \mu_{-1}^2 - \mu_0\mu_{-2} \quad (33)$$

$$B \equiv \mu_0\mu_{-1} - \mu_1\mu_{-2} \quad (34)$$

$$C \equiv \mu_0^2 - \mu_1\mu_{-1} \quad (35)$$

## References and Notes

- (1) Förster, T. *Ann. Phys. (Leipzig)* **1948**, 2, 55.
- (2) Dexter, D. *J. Chem. Phys.* **1953**, 21, 836.
- (3) Szabo, A.; Schulten, K.; Schulten, Z. *J. Chem. Phys.* **1980**, 72, 4350.
- (4) Montroll, E. *J. Math. Phys.* **1969**, 10, 753.
- (5) Hemenger, R.; Pearlstein, R.; Lakatos-Lindenberg, K. *J. Math. Phys.* **1972**, 13, 1056.
- (6) Pearlstein, R. *Photochem. Photobiol.* **1982**, 35, 835.
- (7) Pearlstein, R. *J. Lumin.* **1992**, 51, 139.
- (8) Pullerits, T.; Freiberg, A. *Biophys. J.* **1992**, 63, 879.
- (9) Ermler, U.; Fritzsche, G.; Buchanan, S.; Michel, H. *Structure* **1994**, 2, 925.
- (10) McDermott, G.; Prince, S.; Freer, A.; Hawthornthwaite-Lawless, A.; Papiz, M.; Cogdell, R.; Isaacs, N. *Nature* **1995**, 374, 517.
- (11) Koepke, J.; Hu, X.; Münke, C.; Schulten, K.; Michel, H. *Structure* **1996**, 4, 581.
- (12) Hu, X.; Schulten, K. *Biophys. J.* **1998**, 75, 683.
- (13) Cogdell, R.; Durant, I.; Valentine, J.; Lindsay, J.; Schmidt, K. *Biochim. Biophys. Acta* **1983**, 722, 333.
- (14) Gardiner, A.; Cogdell, R.; Takaichi, S. *Photosyn. Res.* **1993**, 38, 159.
- (15) Hu, X.; Damjanović, A.; Ritz, T.; Schulten, K. *Proc. Natl. Acad. Sci. U.S.A.* **1998**, 95, 5935.
- (16) Hu, X.; Ritz, T.; Damjanović, A.; Schulten, K. *Quart. Rev. Biophys.* **2001**, In press.
- (17) Jimenez, R.; van Mourik, F.; Yu, J. Y.; Fleming, G. R. *J. Phys. Chem. B* **1997**, 101, 7350.
- (18) Leupold, D.; Stiel, H.; Teuchner, K.; Nowak, F.; Sandner, W.; Ucker, B.; Scheer, H. *Phys. Rev. Lett.* **1996**, 77, 4675.
- (19) Monshouwer, R.; Abrahamsson, M.; van Mourik, F.; van Grondelle, R. *J. Phys. Chem. B* **1997**, 101, 7241.
- (20) Pullerits, T.; Chachisvillis, M.; Sundström, V. *J. Phys. Chem.* **1996**, 100, 10787.
- (21) Ray, J.; Makri, N. *J. Phys. Chem. A* **1999**, 103, 9417.
- (22) Hu, X.; Ritz, T.; Damjanović, A.; Schulten, K. *J. Phys. Chem. B* **1997**, 101, 3854.
- (23) Damjanović, A.; Ritz, T.; Schulten, K. *Phys. Rev. E* **1999**, 59, 3293.
- (24) Scholes, G.; Gould, I.; Cogdell, R.; Fleming, G. *J. Phys. Chem. B* **1999**, 103, 2543.
- (25) Mukai, K.; Abe, S.; Sumi, H. *J. Phys. Chem. B* **1999**, 103, 6096.
- (26) Krueger, B. P.; Scholes, G. D.; Fleming, G. R. *J. Phys. Chem. B* **1998**, 102, 5378.
- (27) Ritz, T.; Damjanović, A.; Schulten, K.; Cogdell, R. *J. Phys. Chem. B* **2001**, To be submitted.
- (28) van Grondelle, R.; Dekker, J.; Gillbro, T.; Sundström, V. *Biochim. Biophys. Acta* **1994**, 1187, 1.
- (29) Pullerits, T.; Sundström, V. *Acc. Chem. Res.* **1996**, 29, 381.
- (30) Fleming, G. R.; van Grondelle, R. *Curr. Opin. Struct. Biol.* **1997**, 7, 738.
- (31) Sundström, V.; Pullerits, T.; van Grondelle, R. *J. Phys. Chem. B* **1999**, 103, 2327.
- (32) Ritz, T.; Hu, X.; Damjanović, A.; Schulten, K. *J. Lumin.* **1998**, 76–77, 310.
- (33) Sumi, H. *J. Phys. Chem. B* **1999**, 103, 252.
- (34) Damjanović, A.; Ritz, T.; Schulten, K. *Int. J. Quantum Chem.* **2000**, 77, 139.
- (35) Jungas, C.; Ranck, J.; Rigaud, J.; Joliot, P.; Vermeglio, A. *EMBO J.* **1999**, 18, 534.
- (36) Trissl, H.-W.; Law, C.; Cogdell, R. *Biochim. Biophys. Acta* **1999**, 1412, 149.
- (37) Duysens, L. N. M. *Prog. Biophys. Mol. Biol.* **1964**, 14, 1.
- (38) Frese, R. N.; Olsen, J. D.; Brannvall, R.; Westerhuis, W. H. J.; Hunter, C. N.; van Grondelle, R. *Proc. Natl. Acad. Sci. U.S.A.* **2000**, 97, 5197.
- (39) Papiz, M.; Prince, S.; Hawthornthwaite, A.; McDermott, G.; Freer, A.; Isaacs, N.; Cogdell, R. *Trends in Plant Science* **1996**, 1, 198.
- (40) Law, C.; Cogdell, R.; Trissl, H.-W. *Photosynth. Res.* **1997**, 52, 157.
- (41) Cory, M. G.; Zerner, M. C.; Hu, X.; Schulten, K. *J. Phys. Chem. B* **1998**, 102, 7640.
- (42) Sauer, K.; Smith, J. R. L.; Schultz, A. J. *J. Am. Chem. Soc.* **1966**, 88, 2681.
- (43) Pearlstein, R. M. *Photosynth. Res.* **1992**, 31, 213.
- (44) Ritz, T.; Damjanović, A.; Schulten, K.; Zhang, J.; Koyama, Y. *Photosynth. Res.* **2000**, 66, 125.
- (45) Shreve, A. P.; Trautman, J. K.; Frank, H. A.; Owens, T. G.; Albrecht, A. C. *Biochim. Biophys. Acta* **1991**, 1058, 280.
- (46) Hess, S.; Chachisvillis, M.; Timpmann, K.; Jones, M.; Fowler, G.; Hunter, C.; Sundström, V. *Proc. Natl. Acad. Sci. U.S.A.* **1995**, 92, 12333.
- (47) Visscher, K.; Bergström, H.; Sundström, V.; Hunter, C.; van Grondelle, R. *Photosynth. Res.* **1989**, 22, 211.
- (48) Timpmann, K.; Zhang, F.; Freiberg, A.; Sundström, V. *Biochim. Biophys. Acta* **1993**, 1183, 185.
- (49) Timpmann, K.; Freiberg, A.; Sundström, V. *Chem. Phys.* **1995**, 194, 275.
- (50) Wu, H.-M.; Reddy, N. R. S.; Small, G. J. *J. Phys. Chem. B* **1997**, 101, 651.
- (51) Wu, H.; Small, G. J. *J. Phys. Chem. B* **1998**, 102, 888.
- (52) Damjanović, A.; Kosztin, I.; Schulten, K. *Phys. Rev. E* **2001**, Submitted for publication.
- (53) Cheng, Y. S.; Brantner, C. A.; Tsapin, A.; Collins, M. L. P. *J. Bacteriol.* **2000**, 182, 2100.
- (54) Nadler, W.; Schulten, K. *J. Chem. Phys.* **1985**, 82, 151.
- (55) Humphrey, W. F.; Dalke, A.; Schulten, K. *J. Mol. Graphics* **1996**, 14, 33.